Published in final edited form as:
J Am Coll Cardiol. 2009 April 7; 53(14): 1229–1240. doi:10.1016/j.jacc.2008.12.036.

Imaging Survival and Function of Transplanted Cardiac Resident Stem Cells

Zongjin Li, MD, PhD[*], **Andrew Lee, MS**[*], **Mei Huang, PhD**[*], **Hyung Chun, MD**[†], **Jaehoon Chung, MD**[†], **Pauline Chu, MS**[§], **Grant Hoyt, BS**[‡], **Phillip Yang, MD, PhD**[†], **Jarrett Rosenberg, PhD**[*], **Robert C. Robbins, MD**[‡], and **Joseph C. Wu, MD, PhD**[*,†]

[*] The Department of Radiology and Molecular Imaging Program at Stanford (MIPS), Stanford University School of Medicine, Stanford, CA, USA

[†] Department of Medicine, Division of Cardiology, Stanford University School of Medicine, Stanford, CA, USA

[‡] The Department of Cardiothoracic Surgery, Stanford University School of Medicine, Stanford, CA, USA

[§] The Department of Comparative Medicine, Stanford University School of Medicine, Stanford, CA, USA

Abstract

Objective—The goal of this study is to characterize resident cardiac stem cells (CSCs) and investigate their therapeutic efficacy in myocardial infarction by molecular imaging methods.

Background—CSCs have been isolated and characterized *in vitro.* These cells offer a provocative method to regenerate the damaged myocardium. However, the survival kinetics and function of transplanted CSCs have not been fully elucidated.

Methods—CSCs were isolated from L2G85 transgenic mice (FVB background) that constitutively express both firefly luciferase (Fluc) and enhanced green fluorescence protein (eGFP) reporter gene. CSCs were characterized *in vitro* and transplanted *in vivo* into murine infarction models. Multi-modality noninvasive imaging techniques were used to assess CSC survival and therapeutic efficacy for restoration of cardiac function.

Results—CSCs can be isolated from L2G85 mice and FACS analysis showed expression of resident CSCs markers (Sca-1, c-Kit) and mesenchymal stem cell markers (CD90, CD106). Afterwards, 5×10^5 CSCs (n=30) or PBS control (n=15) was injected into the hearts of syngeneic FVB mice undergoing left anterior descending artery (LAD) ligation. Bioluminescence imaging (BLI) showed poor donor cell survival by week 8. Echocardiogram, invasive hemodynamic pressure-volume (PV) analysis, positron emission tomography (PET) imaging with Fluorine-18-fluorodeoxyglucose ([^{18}F]-FDG), and cardiac magnetic resonance imaging (MRI) demonstrated no significant difference in cardiac contractility and viability between the CSC and control group. Finally, postmortem analysis confirmed transplanted CSCs integrated with host cardiomyocytes by immunohistology.

Correspondence: Joseph C. Wu, MD, PhD, Stanford University School of Medicine, Edwards Building, R354, Stanford, CA 94305-5344, Ph: 650-736-2246, Fax: 650-736-0234, joewu@stanford.edu.

Disclosure. None

Conclusions—In a mouse myocardial infarction (MI) model, Sca-1 positive CSCs provide no long-term engraftment and benefit to cardiac function as determined by multi-modality imaging.

INTRODUCTION

Recent years have brought stem cell therapy for heart disease to the forefront. Several clinical trials have shown beneficial effects of stem cell transplantation to improve cardiac function after myocardial infarction (1–3). However, the mechanism(s) behind this benefit is not clearly understood. Although numerous studies have suggested the cardioprotective benefits from various stem cell types, they also carry limitations including the potential of tumorigenicity with embryonic stem cells (4), arrhythmogenicity with skeletal myoblasts (5), as well as existing controversies surrounding transdifferentation of bone marrow-derived stem cells (6, 7).

The identification of undifferentiated cells with stem cell-like properties derived from the myocardium has renewed the excitement to this field. A number of recent studies have confirmed the presence of cells bearing stem cell markers in the myocardium, which were successfully terminally differentiated into cell lineages that can benefit myocardial function (8–12). A recent study even used resident cardiac stem cells (CSCs) derived from human myocardial biopsy specimen and injected them into mice, showing engraftment and improved myocardial function (12).

We have previously described the L2G85 transgenic mice which constitutively express both the firefly luciferase (Fluc) and enhanced green fluorescence protein (eGFP) genes (13,14). Cells derived from these mice provide the advantage of being “trackable” over time. Using the previously described methods for CSC isolation and proliferation (10), we now provide in detail the survival kinetics of transplanted CSCs in infarcted murine hearts. In contrast to previous studies (9,10,12,15,16), our results suggest that these CSCs do not constitute long-term improvement in myocardial function. We also show definitive evidence via bioluminescence imaging that the majority of these cells are not viable by eight weeks post transplantation.

MATERIALS & METHODS

Isolation and culture of CSCs

Animal protocols were approved by the Stanford University Animal Care and Use Committee. The L2G85 transgenic mice of FVB background with β-actin promoter driving Fluc-eGFP have been described previously (14,17). Normal adult female FVB mice were used as recipient controls. CSCs were isolated from 6 to 12 weeks old L2G85 mice as described with some modifications (10,11,16). In brief, myocardial tissue was cut into 1- to 2-mm piece, washed with Hanks’ balanced salt solution (HBSS) (Invitrogen, Carlsbad, CA), and incubated with 0.1% collagenase II for 30 minutes at 37°C with frequent shaking. Cells were then filtered through 100-μm mesh. The obtained cells were cultured in Iscove’s Modified Dulbecco’s Medium (IMDM) supplemented with 10% fetal bovine serum (FBS) (Hyclone, Logan, UT), 0.1 mM nonessential amino acids, 100 U/mL Penicillin G, 100 μg/mL streptomycin, 2 mmol/L glutamine, and 0.1 mmol/L β-mercaptoethanol. After 2 to 3 weeks, a population of phase-bright cells appeared over the adhered fibroblast-like cells. These phase-bright cells were collected by two washes with PBS, and one wash with cell dissolution buffer (Gibco, Grand Island, NY) at room temperature under microscope monitoring, and sub-cultured in poly-lysine coated plates (BD Biosciences) with the same medium.

Immunofluorescence staining of cultured CSCs

The cells were fixed with 4% paraformaldehyde and processed for immunofluorescence with antibodies to Sca-1 (BD Pharmingen) in situ. Briefly, cells were incubated with rat anti-mouse Sca-1 for 1 hr at room temperature and incubated with goat anti-rat Alexa Fluor 594 (Invitrogen). DAPI was used for nuclear counterstaining.

Flow cytometry analysis

FACS analysis of the bright cells and the cells sub-cultured on poly-lysine coated plates were carried out and the third passage of bone marrow-derived mesenchymal stem cells (BM-MSCs) from L2G85 mice were used as control. The isolation and culturing techniques of BM-MSCs were similar to previous report (18). Antibodies used in this study were phycoerythrin (PE) conjugated anti-CD34, CD29, CD90, CD44, CD54, Allophycocyanin (APC) conjugated anti-CD31 and c-Kit, APC conjugated anti-rat IgG2a, and rat anti-mouse CD62E, CD62P, Tie-2 (all from BD Pharmingen). The stained cells were analyzed using FACS LSR (Becton-Dickinson, MA). Dead cells stained by propidium-iodide (PI) were excluded from the analysis. Isotype-identical antibodies served as controls (BD Pharmingen). FlowJo software (Tree Star Inc, Ashland, OR) was used for followed data analysis.

In vitro differentiation of CSC

For cardiac and smooth muscle differentiation, CSCs were cultured in poly-lysine coated plates in differentiation medium containing 35% IMDM with 10% FBS/65% DMEM–Ham F-12 mix containing 2% B27, 0.1 mmol/L 2-mercaptoethanol, 10 ng/mL epidermal growth factor (EGF; R&D Systems Inc., Minneapolis), 20 ng/mL basic fibroblast growth factor (bFGF; R&D), 40 nmol/L cardiotrophin-1 (R&D), 40 nmol/L thrombin (Sigma-Aldrich, St. Louis), 100 U/mL Penicillin G, 100 μg/mL streptomycin, and 2 mmol/L glutamine (10). After 1 week, the cells were fixed with 4% paraformaldehyde and processed for immunofluorescence with antibodies specific to cardiac troponin T (cTnT), myocyte enhancer factor 2C (MEF-2C), connexin 43, and α-smooth muscle actin (SMA) (all from Santa Cruz Biotech, Santa Cruz, CA) in situ. Briefly, cells were incubated with first antibody for 1 hr at room temperature and incubated with goat anti-rabbit or donkey anti-mouse Alexa Fluor 594. DAPI was used for nuclear counterstaining. For endothelial differentiation, the phase-bright cells were cultured on fibronectin coated plates with EGM-2 (Cambrex, Walkersville, MD) with an extra 20 ng/ml of VEGF. DiI-ac-LDL uptake assay and Matrigel assay were used to confirm endothelial cell phenotype differentiation. For DiI-ac-LDL uptake assay, cells were incubated with 10 μg/ml of DiI-Ac-LDL (Molecular Probes, Eugene, OR) at 37°C for 6 hours. After washing with PBS twice, the slides were fixed and detected with fluorescence microscopy as described (19,20). The formation of endothelial tubes was assessed by seeding cells in 24-well plates coated with Matrigel (BD Pharmingen) and incubating them at 37° for 12 hours as described (19,20). For adipogenic differentiation, the phase-bright cells were cultured in DMEM with 10% FBS, 100 U/mL Penicillin G, 100 μg/mL streptomycin, 2 mmol/L glutamine, 1 μM dexamethasone, 10 μg/ml insulin, 0.5 mM isobulyl-1-methylxanthione, and 200 μM indomethacin for 2 weeks and medium was changed every 3 days. The differentiated adipocytes were confirmed by oil red staining and RT-PCR analysis for peroxisome proliferator-activated receptors gamma (PPARγ) and lipoprotein lipase (LPL) expression. For osteogenic differentiation, the phase-bright cells were cultured in osteogenic differentiation medium (Cambrex, PT-3002) for 2–3 weeks and medium was changed every 3 days. The osteocytes differentiation was confirmed by Alizarin red S staining and RT-PCR analysis for osteocalcin expression as described (21).

Myocardial infarction and cell delivery

All surgical procedures were performed on 8–10 week old female FVB mice (Charles River Laboratories, Inc.) by a single experienced micro-surgeon (GH). FVB mice were anesthetized

with inhaled isoflurane (2% to 3%). Mice were intubated, ventilated, and anesthesia was maintained with inhaled isoflurane (1% to 2.5%). A left thoracotomy was performed and the pericardium was opened. The left anterior descending (LAD) artery was permanently ligated with a 9-0 Ethilon suture just distal to the level of the left atrium. Infarction was visually confirmed by blanching of the anterolateral region of the left ventricle along with dyskinesis. After 30 minutes, 5×10^5 CSCs were injected intramyocardially into the peri-infarct zone at two different sites with a total volume of 20 μl in each animal (n=30). Control animals received PBS injection instead (n=15). For sham operated animals (n=5), open thoracotomy was performed without suturing of the LAD and without injection of CSCs or PBS. A thoracotomy tube was placed and lungs were re-expanded using positive pressure ventilation. The chest cavity was closed in layers with 5-0 Vicryl suture, and the animal was gradually weaned from the respirator. Once spontaneous respiration resumed, the endotracheal and thoracotomy tubes were removed, and the animals were placed in a temperature-controlled chamber until they resumed full alertness and mobility.

Optical bioluminescence imaging (BLI) of transplanted cell survival

BLI was performed on all animals (n=30 CSC, n=15 PBS, and n=5 sham) using the Xenogen IVIS 200 system by a blinded investigator (MH). A majority of the animals were scanned on days 2, 7, 14, 21, 28, 49, and 56. After intraperitoneal injection of the reporter probe D-Luciferin (150 mg/kg), animals were imaged for 1–10 minutes. The same mice were imaged longitudinally for up to 8 weeks. Bioluminescence signal was quantified in units of maximum photons per second per cm square per steridian (photons/sec/cm^2/sr) as described (19).

Cardiac viability with [^{18}F]-FDG positron emission tomography (PET) imaging

Small animal microPET imaging (Vista system, GE Healthcare) was performed in a subset of the animals (n=14 CSC and n=8 PBS) on baseline (day -7) and days 2, 28, and 56 post-operatively. Mice were fasted for 3 hours prior to radioisotope injection. Animals were then injected with 139±23 μCi [^{18}F]-FDG via the tail vein. At 45 to 60 minutes after injection, animals were anesthetized with inhaled 2% isoflurane. Images were performed, reconstructed by filtered back projection (FBP), and analyzed using image software Amide (http://amide.sourceforge.net/index.html) by blinded investigator (AL). Three-dimensional regions of interest (ROIs) were drawn encompassing the heart. For each ROI, counts/ml/min were then converted to counts/gram/min and divided by the injected dose to obtain the image ROI derived [^{18}F]-FDG percentage injected dose per gram of heart (% ID/g) as described (22). To measure the myocardium infarction size, [^{18}F]-FDG PET images were assembled into polar maps (23). The size of perfusion defects was measured as the myocardium with 50% of maximum activity and expressed as percent total myocardium polar map by GE Healthcare Advantage Workstation (GE Healthcare, UK).

Left ventricular functional analysis with echocardiogram and pressure-volume (PV) acquisition

Echocardiography was performed in all animals (n=30 CSC, n=15 PBS, and n=5 sham). A majority of the animals were scanned on baseline (day -7) and days 2, 28, and 56 post-operatively by a blinded investigator (MH) using the Siemens-Acuson Sequoia C512 system equipped with a multi-frequency (8–14 MHz) 15L8 transducer. Animals were anesthetized with inhaled 2% isoflurane. Analysis of M-mode images was performed. Left ventricular end diastolic diameter (LVEDd) and end-systolic diameter (LVESd) were measured and used to calculate fractional shortening (FS) by the following formula: FS= [LVEDd-LVESd]/LVEDd. At the end of the study (week 8), invasive hemodynamic measurements were performed in a subset of the animals (n=5/group for CSC, PBS, and sham) as described (24). Briefly, after midline neck incision, a conductance 1.4 conductance catheter (Millar Instruments, Houston,

TX, USA) was introduced into the left ventricle through the right carotid artery. After stabilization, the signals were continuously recorded at a sampling rate of 1000/s using pressure-volume conductance system coupled to a PowerLab/4SP analog to digital converter (ADInstruments). Data were analyzed by using a cardiac pressure-volume analysis program (PVAN 3.4; Millar Instruments, Houston, TX, USA) and Chart/Scope Software (AD Instruments, Colorado Springs, CO, USA).

Assessment of cardiac contractility with MRI

Please see Supplemental Methods.

Histological analysis

After completion of the imaging protocols, all animals were sacrificed at week 8. For immunostaining, explanted hearts (n=10 for CSC, n=5 for PBS, and n=2 for sham) were embedded into OCT compound (Miles Scientific), snap frozen in liquid nitrogen, and cut into transverse sections at 5 μm thickness. To track GFP positive CSC-derived cells and cardiomyocytes differentiation in hearts, anti-GFP antibody (Invitrogen) and anti-α-sarcomeric actin (α-SA) antibody (Sigma) were used. Alexa Fluor 488 and Alexa Fluor 594-conjugated secondary antibodies were applied appropriately. DAPI was used for nuclear counterstaining. To detect microvascular density (MVD) in the peri-infarct area, a rat anti-mouse CD31 (BD Pharmingen) and Alexa Fluor 647-conjugated secondary antibody were used. The number of capillary vessels was counted by a blinded investigator (HC) in ten randomly selected areas using a fluorescence microscope (200x magnification). To detect fibrosis in cardiac muscles, explanted hearts (n=10 for CSC, n=5 for PBS, and n=2 for sham) were fixed in 4% paraformaldehyde, cut transversely, embedded in paraffin, and stained with Masson's trichome (25). Five to six sections from apex to base were subjected to staining. Images of each section were taken to calculate the fibrotic and nonfibrotic areas as well as ventricular and septal wall thickness. The thinning index is a ratio of the amount of wall thinning in the infarct normalized to the thickness of the septum and is calculated by dividing the minimal infarct wall thickness with maximal septal wall thickness. The measurement of area of fibrosis and thinning index were determined by Image J software (NIH) performed on 3 separate sections, and the averages were used for statistical analysis.

Statistical analysis

Comparison of fractional shortening (FS), ejection fraction (EF), cardiac viability, and infarction size between CSC and sham/PBS groups over time was done by two-way repeated measures ANOVA with group and day as factors, using a Greenhouse-Geisser correction for lack of sphericity. Comparison of end systolic and diastolic volume and pressure between CSC and sham/PBS groups was done by two-way repeated measures ANOVA with group and cardiac phase as factors, using a Greenhouse-Geisser correction for lack of sphericity. Comparison of histological infarct size and microvascular density between PBS and CSC groups was done by two-tailed t-test. Statistics were calculated using SPSS 14.0 (SPSS Inc., Chicago, IL, USA). Descriptive statistics included mean and standard error. Differences were considered significant at P values of <0.05.

Statement of Responsibility

The authors had full access to and take full responsibility for the integrity of the data. All authors have read and accept the manuscript as written.

RESULTS

Isolation and culturing of cardiac stem cells (CSCs)

Explanted hearts were subjected to enzymatic digestion, cultured, and are composed of Sca-1 positive cells (Figure 1A). Phase bright spherical cells that spontaneously separated from the myocardium samples were identified after 2–3 weeks. These cells demonstrated a high nucleus to cytoplasm ratio and expressed robust GFP (Figure 1B). Importantly, assessment of Fluc expression showed a linear correlation (r^2=0.98) between the total cell numbers and the bioluminescence signals (Figure 1C), which is needed for accurate tracking of cell fate in subsequent *in vivo* imaging studies. The cells also demonstrated linear growth with population doubling time of approximately 5 days (Figure 1D), similar to previous studies (10,12,16).

Characterization of surface markers in cardiac stem cells

Previous studies have shown that Sca-1 expressing cells possess the potential to differentiate into cardiomyocytes (10,11). Our results showed that ~35.0±5.5% of the phase-bright cells were Sca-1 positive. After subculturing for 1–2 weeks, Sca-1 expression on CSCs was up-regulated close to 95% (Figure 2A). In order to further characterize their cellular phenotypes, detailed flow cytometry analysis was performed. Overall, the subcultured group had higher expression of mesenchymal stem cell markers (CD29, CD90, CD44, CD106), but endothelial (CD31, CD34, CD44) and c-Kit markers were both down-regulated (Figure 2B). Interestingly, compared to BM-MSCs, sub-cultured CSCs have similar expression pattern but express higher CD29 and CD90 and lower CD54. CSCs isolated from normal syngeneic FVB mice also showed similar results (data not shown), suggesting no significant effects on cellular characteristics from the stable expression of Fluc-eGFP reporter gene. Overall, the expression of these markers in our CSCs are similar to previously published data (12,26).

Multipotent differentiation of CSCs

We next examined the differentiation of CSCs into various cell types. Similar to other studies (10,21,27,28), these cells can differentiate into cardiomyocytes and smooth muscle cells, as documented by positive staining for cardiac troponin T (cTnT), connexin 43, MEF-2C, and α-smooth muscle actin (Figure 3A). After seven days in differentiation medium, the cells developed into clusters, and after two weeks they formed into spherical collection of cells, some of which showed spontaneous contractility (Supplementary Video). In addition, these cells were capable of differentiating into endothelial cells as demonstrated by DiI-ac-LDL uptake and Matrigel angiogenesis assays (Figure 3B), into adipocytes as demonstrated by oil red staining and RT-PCR analysis (Figure 3C), and into osteoblasts as demonstrated by Alizarin Red S staining and RT-PCR analysis (Figure 3D).

Injection of CSCs into infarcted myocardium

Several groups have reported that CSCs can proliferate indefinitely *in vitro* (10,21,27,28). This begs the question whether CSCs can have similar growth properties *in vivo*, and if so, whether this could lead to potential tumorigenesis. In order to address this question, adult FVB mice were subjected to LAD artery ligation followed by injection with either 5×10^5 cultured CSCs (n=30) or PBS (n=15). Injection of CSCs into infarcted myocardium resulted in a robust bioluminescence signal at day 2. However, serial imaging of the same animals out to 8 weeks demonstrated a significant decay in the bioluminescence signal. When normalized to results from day 2, the percent bioluminescence signals were 6.7±0.5 at day 7, 3.9±0.8 at day 14, 1.7 ±0.2 at day 21, 1.4±0.1 at day 28, and 0.4±0.1 at day 56 (Figure 4). Control animals injected with PBS showed no imaging signals as expected.

Assessment of cardiac contractility and hemodynamic status following CSC therapy

To date, only a few studies have demonstrated that CSC can improve cardiac function (10, 21,27,28). In order to confirm these results, echocardiograms were performed at baseline, day 2, day 28, and day 56 post surgery (Figure 5A, B). At day 2 following infarction, there was a significant decrease in the fractional shortening (FS) in both the CSC group and PBS group compared to the baseline, consistent with successful induction of myocardial infarction. At day 28 and day 56, there was trend toward slight improvement in the FS for both groups, but the difference was not statistically significant. These results were also confirmed in a subset of the animals that underwent cardiac MRI which showed no functional change in ejection fraction (EF) (Supplemental Figure 1). In addition, invasive hemodynamic parameters showed decrease in EF for both CSC and control groups compared to sham group (Supplemental Figure 2). This was associated with higher left ventricular end diastolic volume (EDV) and left ventricular end systolic volume (ESV) in both groups compared to sham. Finally, as highlighted in Supplemental Table 2, there was no significant difference in other functional parameters (e.g., cardiac output, stroke volume) between CSC transplanted mice and PBS control mice.

Assessment of cardiac viability following CSC therapy

In addition, we performed [^{18}F]-FDG PET scans of the mice at baseline, day 2, day 28, and day 56 post surgery. This technique can be used to detect changes in cardiac viability following interventions in small animal models (29). At day 2 following infarction, there was a significant reduction in cardiac viability for both groups (20.2±4.9 %ID/g for PBS and 20.8±4.2 %ID/g for CSCs; $P<0.001$), consistent with successful induction of myocardial infarction. However, at day 28 and day 56, there was no significant difference between the treatment arm and control group (Figure 6A,B). Moreover, analysis of the [^{18}F]-FDG PET images using polar-map reconstruction revealed no significant difference of infarction size between the CSC transplantation group and the PBS group (Figure 6C,D).

Histologic assessment of infarct size and CSC engraftment

Histologic analysis of the myocardium was performed by both looking at thin sections of the gross specimen and via immunofluorescent microscopic examination. Microscopic examination showed the presence of GFP positive cells within myocardium at day 3 (Figure 7A–B). At day 14, CSCs could differentiate into cardiomyocytes as confirmed by α-SMA and GFP double stainings (Figure 7C). However, this population became significantly decreased when the tissues were examined at day 28 (Figure 7D), which is also consistent with the decrease in bioluminescence signals over this period of time (Figure 4). Finally, examination of the explanted hearts showed no significant difference in the infarct size and microvascular density (MVD) between the two groups (Supplemental Figure 3).

DISCUSSION

In this study, we isolated cardiac resident stem cells from L2G85 transgenic mice that constitutively expressed Fluc-eGFP, enabling us to track stem cell by both noninvasive imaging and invasive histopathology. Upon culturing, we demonstrated that these phase-bright cells upregulated Sca-1 and expressed surface markers resembling mesenchymal stem cells. We also present evidence that molecular imaging can be used to track CSCs survival in a murine model of myocardial infarction. When injected directly into the infarcted heart, these cells initially demonstrated viability by bioluminescence imaging. But after a period of eight weeks, the majority of the imaging signals were no longer present, suggesting elimination from the myocardium. Consequently, we found no significant physiologic benefit from CSC therapy as determined from multiple parameters, including fractional shortening by echocardiogram, myocardial glucose uptake by [^{18}F]-FDG PET scan, ejection fraction by MRI, invasive PV loop analysis, and infarct size by histopathologic assessment.

Recent works have documented the presence of a reservoir of stem and progenitor cells in the myocardium (8,10,16,21,30–32). These cells have been successfully isolated and expanded *ex vivo*, and have been differentiated into cardiomyocytes, smooth muscle cells, and endothelial cells (10,16,21,26,30–32). Previous works using CSCs have also demonstrated significant improvement in cardiac function after CSC injection, which was in part attributed to the persistent engraftment of the injected CSCs into the infarct zone (9,12,16,33). Higher percentage of viable myocardium within the infarct zone and improved ejection fraction were demonstrated up to five weeks after cell transplantation (9). In contrast, bioluminescence imaging data from our study suggests that by week 8, <0.5% of the transplanted CSCS are still alive. By echocardiography and PET imaging, no significant changes were observed at day 28 and day 56 in cardiac contractility and viability.

At present, we can only speculate that the discrepancy in findings may be attributed to *differences* in isolation techniques (cardiosphere, side population), stem cell marker expression (c-Kit, Sca-1), donor cell sources (human, mice), particular strains of mice used, or host animal models (non-reperfused LAD ligation, ischemia-reperfusion) (34). From the procedural standpoint, we can not exclude that the possibility that our mice may have been oversedated (2% isoflurane) given the lower baseline fractional shortening values (35–40%) observed compared to previous studies (35). This could have undermined the chances of detecting a small but significant change between the two groups. From the transgenic model standpoint, it is possible that Fluc reporter gene silencing may have occurred and limited our ability to detect surviving CSCs at late time points. However, a previous study using hematopoietic stem cells isolated from these mice was able to demonstrate complete reconstitution of the irradiated bone marrow at late time points as detected by BLI, which argues against significant transgene silencing (17). From the technical standpoint, BLI is limited to small animal imaging as the low energy photons (2–3 eV) can become attenuated within deeper tissues (e.g., heart) compared with more superficial locations (e.g., skeletal muscles). At present, a conservative estimate of minimal detectable cell number by BLI is ~1,000 in the heart vs. ~100 in the leg (14). Finally, from the instrumentation standpoint, it is plausible that the image resolution (~1.5 mm^3) and detection sensitivity (10^{-9} to 10^{-12} molar) of the small animal microPET scanner is still insufficient to distinguish subtle but significant differences in [^{18}F]-FDG uptake between the two groups. Thus, additional studies will be needed in the future to further examine each of these variables separately.

Just as the mechanism of stem cells exerting benefit on myocardial function remains to be fully elucidated, the mechanism of their elimination over time also remains poorly understood. The pattern of acute donor cell death seen in our CSC transplantation is also consistent with previous studies showing poor donor cell survival after transplantation of neonatal cardiomyocytes (36), mesenchymal stem cells (37), bone marrow mononuclear cells (14), and human embryonic stem cell-derived cardiomyocytes (38). A number of culprits may be involved, including inflammation, ischemia, apoptosis, anoikis, and autophagy may all play contributory roles. Furthermore, the myocardial milieu *in vivo* is a stark contrast to the rich nutrients and oxygen concentration that have been optimized for their cell culturing, growth, and expansions *in vitro*. It is interesting to note historically that myoblast transplantation as a potential cell-based therapy for patients with Duchenne muscular dystrophy (DMD) met with disappointing failures in the 1990s (39). One of the main reasons was acute donor cell death following transplantation. Future clinical studies aimed at transplanting CSCs in patients will likely need to first understand the mechanism of acute donor cell death.

Despite the limitation of acute donor stem cell death, both animal and clinical studies have suggested beneficial effects following transplantation of various stem cell types (40), perhaps acting through paracrine pathways (41). Thus, strategies aimed at prolonging cell survival (and hence prolonging paracrine activation) may lead to even more favorable results. To that extent,

the application of bioengineering methods (42) or pro-survival cocktails (43) or genetic modification (44), rather than direct stem cell injection, may prove to be a more viable approach for achieving long-term engraftment in the future. Encouragingly, recent study by Tillmanns *et al*. showed that CSCs activated with insulin-like growth factor 1 and hepatocyte growth factor before their injection into infarcted sites had significantly improved cell survival rate and was able to form conductive arterioles and capillaries in the host myocardium (45).

In summary, our study demonstrates that imaging can be used to monitor CSC fate noninvasively in living animals and that CSC transplantation provides no significant benefits to cardiac function in a mouse myocardial infarction model. As the field of cardiac stem cell therapy continues to mature, it is critical to better understand the underlying mechanism of the treatment modality, and to identify the potential pitfalls of the therapy prior to its incorporation into the clinical realm (1). Although a stem cell source from the heart is of tremendous potential, cautious optimism is necessary prior to full clinical use of these cells.

Supplementary Material

Refer to Web version on PubMed Central for supplementary material.

Acknowledgments

This work was supported in part by grants from the NIH HL089027 (JCW), Burroughs Wellcome Foundation Career Award for Medicine Scientists (JCW), and Society of Nuclear Medicine Pilot Research Award (ZL).

References

1. Rosenzweig A. Cardiac cell therapy--mixed results from mixed cells. N Engl J Med 2006;355:1274–7. [PubMed: 16990391]
2. Assmus B, Honold J, Schachinger V, et al. Transcoronary transplantation of progenitor cells after myocardial infarction. N Engl J Med 2006;355:1222–32. [PubMed: 16990385]
3. Wollert KC, Meyer GP, Lotz J, et al. Intracoronary autologous bone-marrow cell transfer after myocardial infarction: the BOOST randomised controlled clinical trial. Lancet 2004;364:141–8. [PubMed: 15246726]
4. Cao F, Lin S, Xie X, et al. In vivo visualization of embryonic stem cell survival, proliferation, and migration after cardiac delivery. Circulation 2006;113:1005–14. [PubMed: 16476845]
5. Menasche P, Alfieri O, Janssens S, et al. The Myoblast Autologous Grafting in Ischemic Cardiomyopathy (MAGIC) trial: first randomized placebo-controlled study of myoblast transplantation. Circulation 2008;117:1189–200. [PubMed: 18285565]
6. Balsam LB, Wagers AJ, Christensen JL, Kofidis T, Weissman IL, Robbins RC. Haematopoietic stem cells adopt mature haematopoietic fates in ischaemic myocardium. Nature 2004;428:668–73. [PubMed: 15034594]
7. Orlic D, Kajstura J, Chimenti S, et al. Bone marrow cells regenerate infarcted myocardium. Nature 2001;410:701–5. [PubMed: 11287958]
8. Beltrami AP, Barlucchi L, Torella D, et al. Adult cardiac stem cells are multipotent and support myocardial regeneration. Cell 2003;114:763–76. [PubMed: 14505575]
9. Dawn B, Stein AB, Urbanek K, et al. Cardiac stem cells delivered intravascularly traverse the vessel barrier, regenerate infarcted myocardium, and improve cardiac function. Proc Natl Acad Sci U S A 2005;102:3766–71. [PubMed: 15734798]
10. Messina E, De Angelis L, Frati G, et al. Isolation and expansion of adult cardiac stem cells from human and murine heart. Circ Res 2004;95:911–21. [PubMed: 15472116]
11. Oh H, Bradfute SB, Gallardo TD, et al. Cardiac progenitor cells from adult myocardium: homing, differentiation, and fusion after infarction. Proc Natl Acad Sci U S A 2003;100:12313–8. [PubMed: 14530411]

12. Smith RR, Barile L, Cho HC, et al. Regenerative potential of cardiosphere-derived cells expanded from percutaneous endomyocardial biopsy specimens. Circulation 2007;115:896–908. [PubMed: 17283259]
13. Chang GY, Cao F, Krishnan M, et al. Positron emission tomography imaging of conditional gene activation in the heart. J Mol Cell Cardiol 2007;43:18–26. [PubMed: 17467733]
14. Sheikh AY, Lin SA, Cao F, et al. Molecular imaging of bone marrow mononuclear cell homing and engraftment in ischemic myocardium. Stem Cells 2007;25:2677–84. [PubMed: 17628019]
15. Gonzalez A, Rota M, Nurzynska D, et al. Activation of Cardiac Progenitor Cells Reverses the Failing Heart Senescent Phenotype and Prolongs Lifespan. Circ Res 2008;102:597–606. [PubMed: 18202313]
16. Ott HC, Matthiesen TS, Brechtken J, et al. The adult human heart as a source for stem cells: repair strategies with embryonic-like progenitor cells. Nat Clin Pract Cardiovasc Med 2007;4 (Suppl 1):S27–39. [PubMed: 17230213]
17. Cao YA, Wagers AJ, Beilhack A, et al. Shifting foci of hematopoiesis during reconstitution from single stem cells. Proc Natl Acad Sci U S A 2004;101:221–6. [PubMed: 14688412]
18. Sun S, Guo Z, Xiao X, et al. Isolation of mouse marrow mesenchymal progenitors by a novel and reliable method. Stem Cells 2003;21:527–35. [PubMed: 12968107]
19. Li Z, Wu JC, Sheikh AY, et al. Differentiation, survival, and function of embryonic stem cell derived endothelial cells for ischemic heart disease. Circulation 2007;116:I46–54. [PubMed: 17846325]
20. Li ZJ, Wang ZZ, Zheng YZ, et al. Kinetic expression of platelet endothelial cell adhesion molecule-1 (PECAM-1/CD31) during embryonic stem cell differentiation. J Cell Biochem 2005;95:559–70. [PubMed: 15786495]
21. Matsuura K, Nagai T, Nishigaki N, et al. Adult cardiac Sca-1-positive cells differentiate into beating cardiomyocytes. J Biol Chem 2004;279:11384–91. [PubMed: 14702342]
22. Toyama H, Ichise M, Liow JS, et al. Evaluation of anesthesia effects on [18F]FDG uptake in mouse brain and heart using small animal PET. Nucl Med Biol 2004;31:251–6. [PubMed: 15013491]
23. Kudo T, Fukuchi K, Annala AJ, et al. Noninvasive measurement of myocardial activity concentrations and perfusion defect sizes in rats with a new small-animal positron emission tomograph. Circulation 2002;106:118–23. [PubMed: 12093780]
24. Xu M, Uemura R, Dai Y, Wang Y, Pasha Z, Ashraf M. In vitro and in vivo effects of bone marrow stem cells on cardiac structure and function. J Mol Cell Cardiol 2007;42:441–8. [PubMed: 17187821]
25. Engel FB, Hsieh PC, Lee RT, Keating MT. FGF1/p38 MAP kinase inhibitor therapy induces cardiomyocyte mitosis, reduces scarring, and rescues function after myocardial infarction. Proc Natl Acad Sci U S A 2006;103:15546–51. [PubMed: 17032753]
26. Tateishi K, Ashihara E, Honsho S, et al. Human cardiac stem cells exhibit mesenchymal features and are maintained through Akt/GSK-3beta signaling. Biochem Biophys Res Commun 2007;352:635–41. [PubMed: 17150190]
27. Barile L, Chimenti I, Gaetani R, et al. Cardiac stem cells: isolation, expansion and experimental use for myocardial regeneration. Nat Clin Pract Cardiovasc Med 2007;4 (Suppl 1):S9–S14. [PubMed: 17230222]
28. Bearzi C, Rota M, Hosoda T, et al. Human cardiac stem cells. Proc Natl Acad Sci U S A 2007;104:14068–73. [PubMed: 17709737]
29. Schelbert HR, Inubushi M, Ross RS. PET imaging in small animals. J Nucl Cardiol 2003;10:513–20. [PubMed: 14569245]
30. Lyngbaek S, Schneider M, Hansen JL, Sheikh SP. Cardiac regeneration by resident stem and progenitor cells in the adult heart. Basic Res Cardiol 2007;102:101–14. [PubMed: 17216393]
31. Oyama T, Nagai T, Wada H, et al. Cardiac side population cells have a potential to migrate and differentiate into cardiomyocytes in vitro and in vivo. J Cell Biol 2007;176:329–41. [PubMed: 17261849]
32. Rosenblatt-Velin N, Lepore MG, Cartoni C, Beermann F, Pedrazzini T. FGF-2 controls the differentiation of resident cardiac precursors into functional cardiomyocytes. J Clin Invest 2005;115:1724–33. [PubMed: 15951838]

33. Tateishi K, Ashihara E, Takehara N, et al. Clonally amplified cardiac stem cells are regulated by Sca-1 signaling for efficient cardiovascular regeneration. J Cell Sci 2007;120:1791–800. [PubMed: 17502484]
34. Garry DJ, Martin CM. Cardiac regeneration: self-service at the pump. Circ Res 2004;95:852–4. [PubMed: 15514166]
35. McLaughlin L, Zhu G, Mistry M, et al. Apolipoprotein J/clusterin limits the severity of murine autoimmune myocarditis. J Clin Invest 2000;106:1105–13. [PubMed: 11067863]
36. Zhang M, Methot D, Poppa V, Fujio Y, Walsh K, Murry CE. Cardiomyocyte grafting for cardiac repair: graft cell death and anti-death strategies. J Mol Cell Cardiol 2001;33:907–21. [PubMed: 11343414]
37. van der Bogt KE, Sheikh AY, Schrepfer S, et al. Comparison of different adult stem cell types for treatment of myocardial ischemia. Circulation 2008;118:S121–9. [PubMed: 18824743]
38. Cao F, Wagner RA, Wilson KD, et al. Transcriptional and functional profiling of human embryonic stem cell-derived cardiomyocytes. PLoS ONE 2008;3:e3474. [PubMed: 18941512]
39. Mendell JR, Kissel JT, Amato AA, et al. Myoblast transfer in the treatment of Duchenne's muscular dystrophy. N Engl J Med 1995;333:832–8. [PubMed: 7651473]
40. Wollert KC, Drexler H. Clinical applications of stem cells for the heart. Circ Res 2005;96:151–63. [PubMed: 15692093]
41. Gnecchi M, He H, Liang OD, et al. Paracrine action accounts for marked protection of ischemic heart by Akt-modified mesenchymal stem cells. Nat Med 2005;11:367–8. [PubMed: 15812508]
42. Cao F, Sadrzadeh Rafie AH, Abilez OJ, et al. In vivo imaging and evaluation of different biomatrices for improvement of stem cell survival. J Tissue Eng Regen Med 2007;1:465–8. [PubMed: 18163533]
43. Laflamme MA, Chen KY, Naumova AV, et al. Cardiomyocytes derived from human embryonic stem cells in pro-survival factors enhance function of infarcted rat hearts. Nat Biotechnol 2007;25:1015–24. [PubMed: 17721512]
44. Muraski JA, Rota M, Misao Y, et al. Pim-1 regulates cardiomyocyte survival downstream of Akt. Nat Med 2007;13:1467–75. [PubMed: 18037896]
45. Tillmanns J, Rota M, Hosoda T, et al. Formation of large coronary arteries by cardiac progenitor cells. Proc Natl Acad Sci U S A 2008;105:1668–73. [PubMed: 18216245]

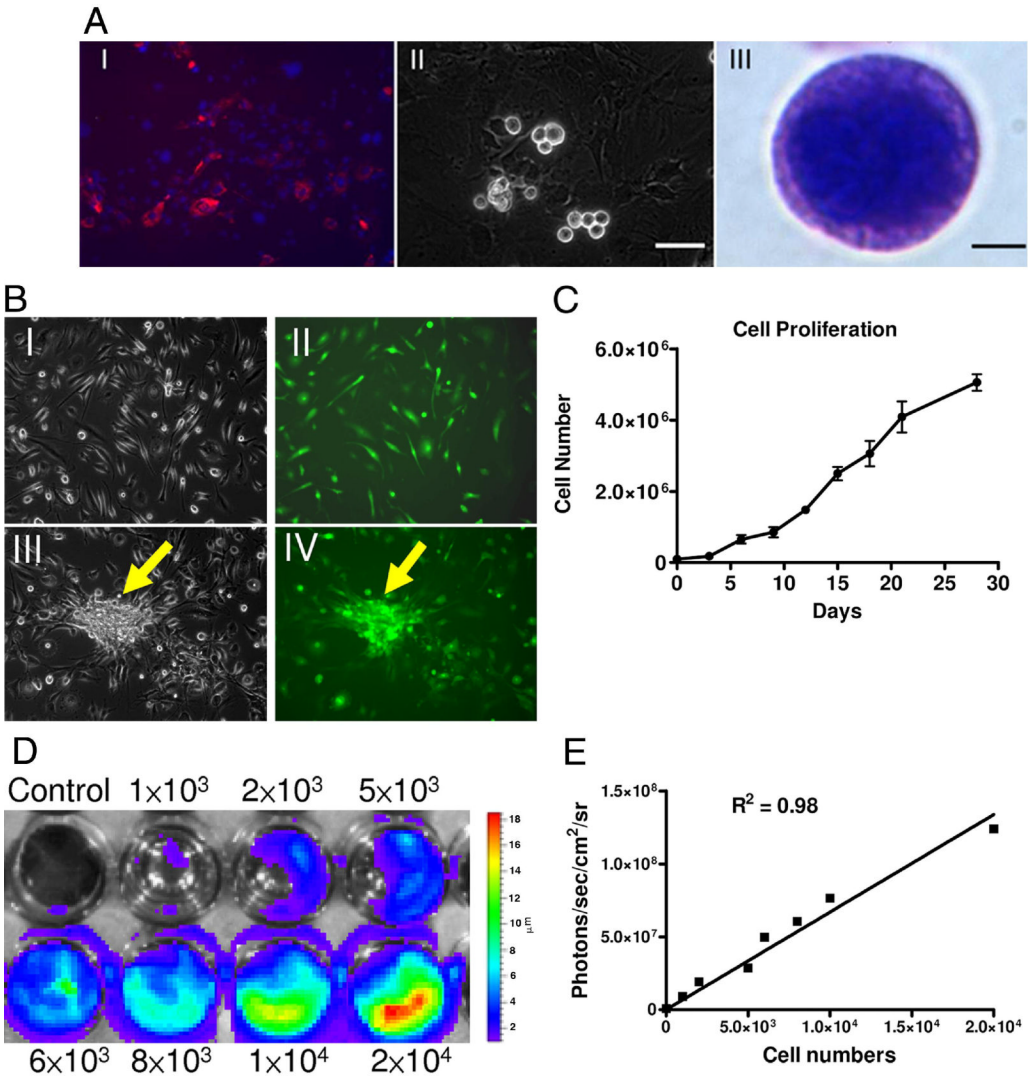

Figure 1. Isolation and culturing of cardiac stem cells

(A) Ventricular cells from L2G85 transgenic mice stained for Sca-1 (red) **(I)**. After a period ranging from 1 to 3 weeks, phase-bright cells migrated over a layer of fibroblast-like cells **(II)**. The phase-bright cells were collected and Giemsa stain showed the cell with large nucleus **(III)**. Scale bar=50μm (i, ii), 2μm (III). **(B)** Subculture and *in vitro* differentiation of phase-bright cells. Morphology of CSCs **(I)** cultured in poly-D-lysine-coated plates and expressing GFP **(II)**. With cardiac differentiation medium, some CSCs can form cardiac sphere (arrow) with GFP expression **(III, IV). (C)** Proliferation curves show linear growth of cultured CSCs over a one month period. **(D) & (E)** *Ex vivo* imaging analysis of CSCs show increasing bioluminescence signals with cell numbers (r^2=0.98)

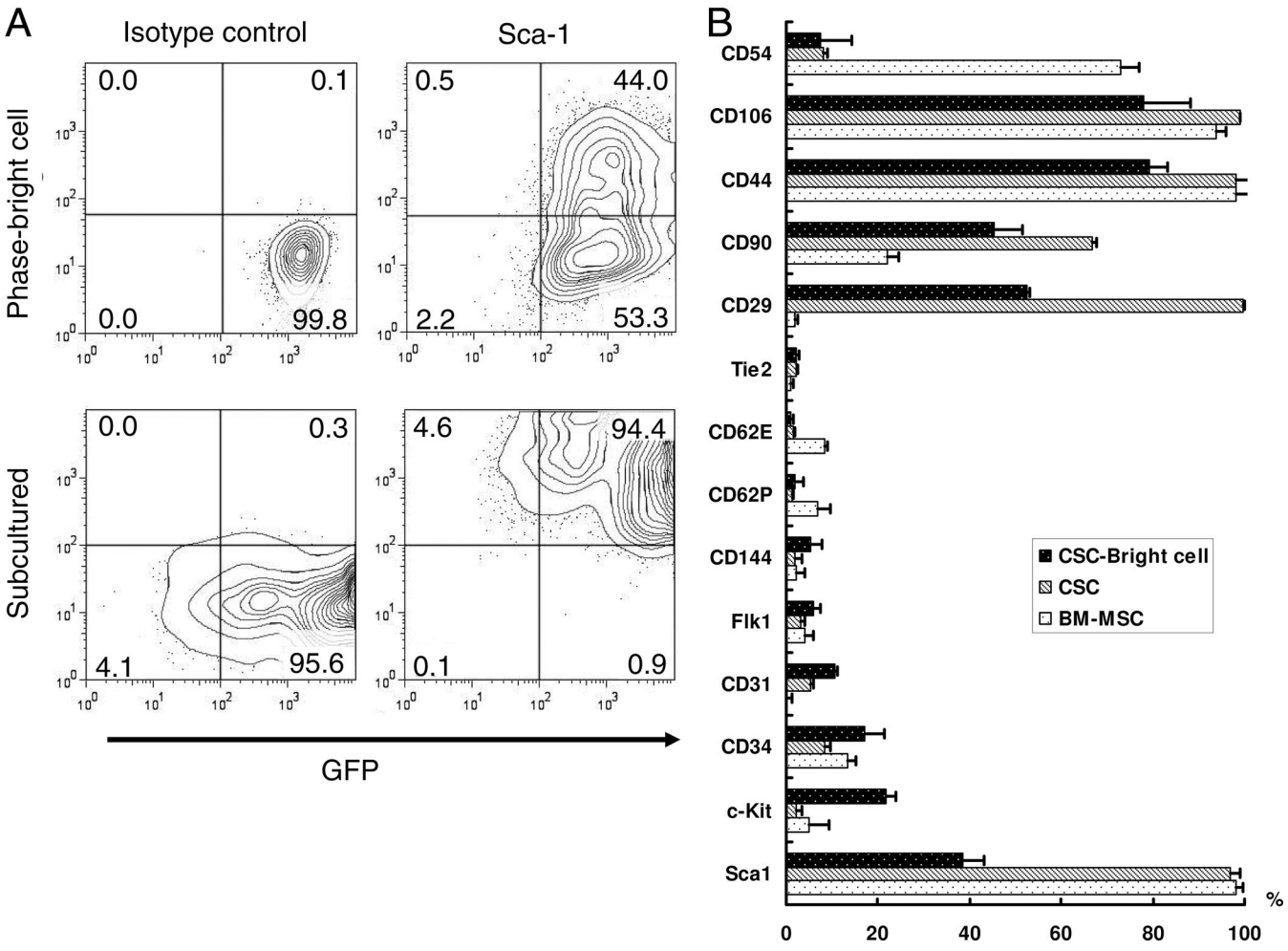

Figure 2. Characterization of surface markers in cardiac stem cells

Quantification by FACS analysis of CSC phase-bright cells and its derived cells. Bone marrow mononuclear cells derived mesenchymal stem cells (BM-MSC) were used as control. **(A)** CSCs express robust GFP both on phase-bright CSCs and their subcultures. After 2–3 passages, there was upregulation of Sca-1. Lower panels showed Sca-1 antibody isotype control. **(B)** Quantitative analysis of cell markers expression by FACS. CSCs express high level mesenchymal stem cells markers, CD29, CD90, CD44, and CD106. After subculturing, Sca-1 up-regulated but c-Kit, CD34, CD31, and CD144 markers all down-regulated. Compare to BM-MSC, CSCs express less CD54, but higher CD29 and CD90. All FACS experiments were performed in triplicates.

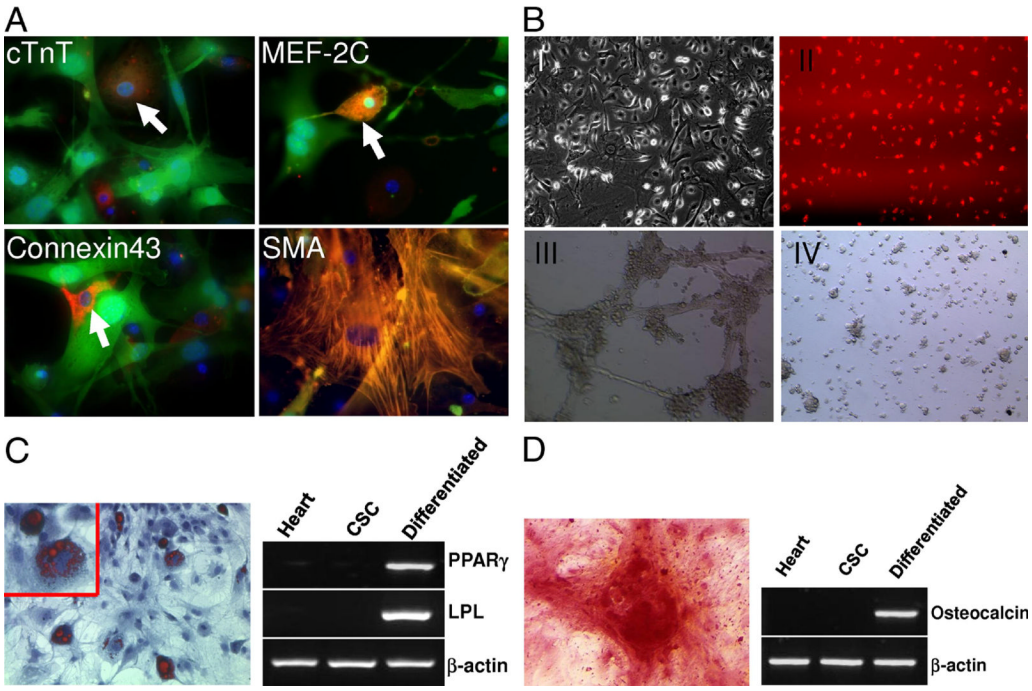

Figure 3. Multipotent capacity of cardiac stem cells

(A) Cardiac and smooth muscle differentiation of CSCs *in vitro*. Immunostaining of GFP positive CSCs with cardiac troponin T (cTnT), myocyte enhancer factor 2C (MEF-2C), connexin-43, and α-smooth muscle actin (α-SMA). **(B)** Endothelial differentiation of CSCs *in vitro*. The cells were cultured in EGM-2 medium with 10 ng/ml VEGF and showed endothelial differentiation by morphology **(I)** and uptake of Dil-ac-LDL **(II)**. Endothelial tube formation by differentiated CSCs after 12 hours of plating on Matrigel **(III)** whereas undifferentiated CSCs cells do not form cord-like structures **(IV)**. **(C)** Oil red staining and RT-PCR analysis of PPARγ and lipoprotein lipase (LPL) expression shows adipogenic differentiation of the CSCs induced for 2 weeks. **(D)** Alizarin red S staining of calcium and RT-PCR analysis of osteocalcin expression shows CSCs induced to differentiate into osteoblasts.

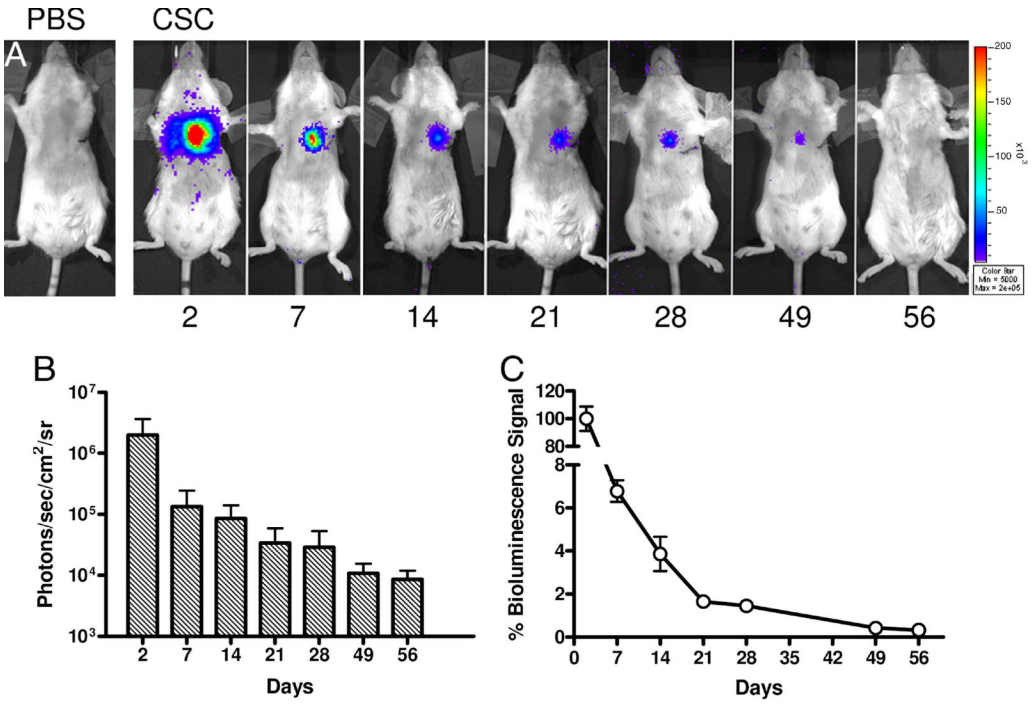

Figure 4. Reporter gene imaging of CSCs fate after transplantation

(A) A representative animal injected with 5×10^5 CSCs shows significant bioluminescence activity at day 2, which decreases progressively over the following 8 weeks. **(B)** Detailed quantitative analysis of signals from all animals transplanted with CSCs. Signal activity is expressed as photons/sec/cm^2/sr. **(C)** Estimation of percent donor cell survival plotted as % signal activity (normalized to day 2) over the 8 week period following transplantation.

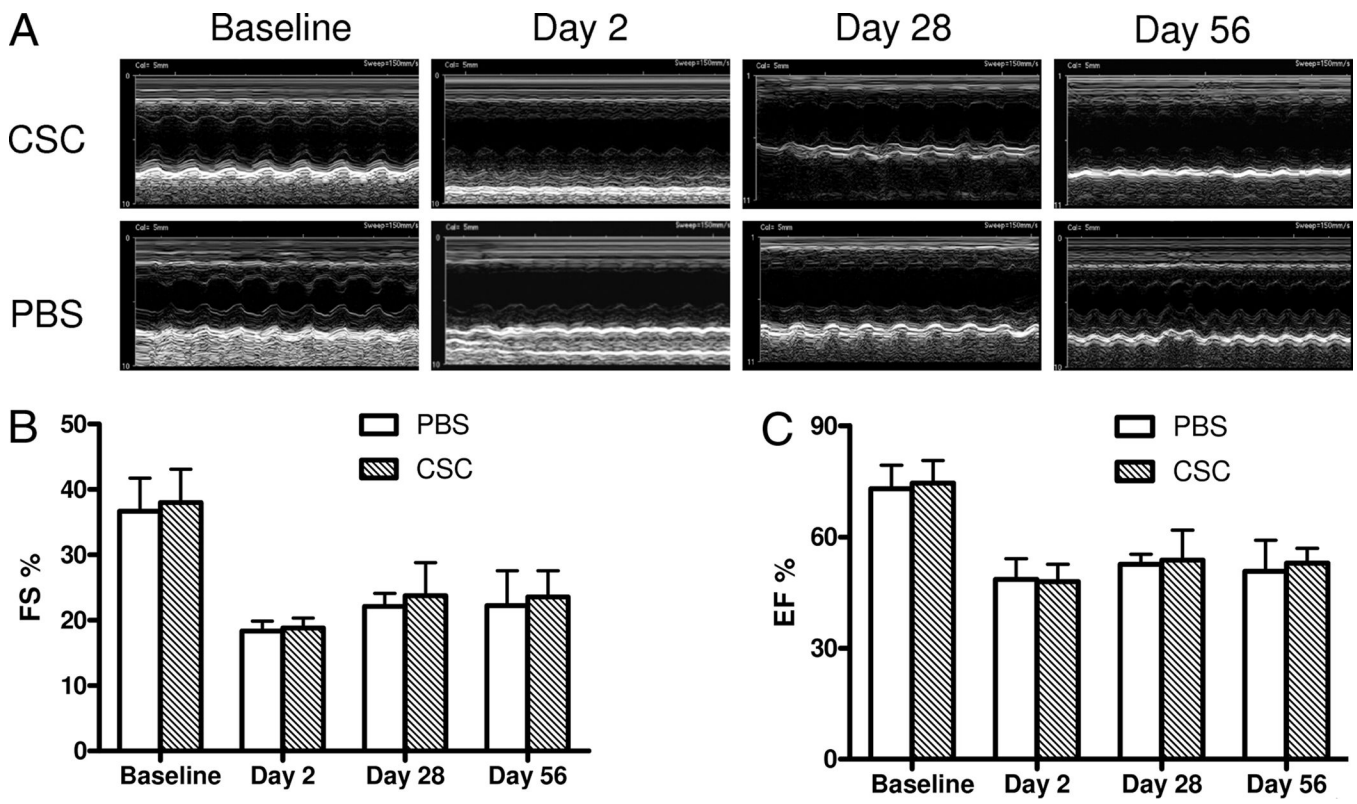

Figure 5. Echocardiographic evaluation of cardiac contractility

(A) Representative M-mode echocardiographic data of infarcted hearts receiving PBS vs. CSCs at day 2, week 4, and week 8. **(B,C)** Comparison of fractional shortening (FS) and ejection fraction (EF) between the two groups 7 days before (baseline), 2 days, 28 days, and 56 days after LAD ligation.

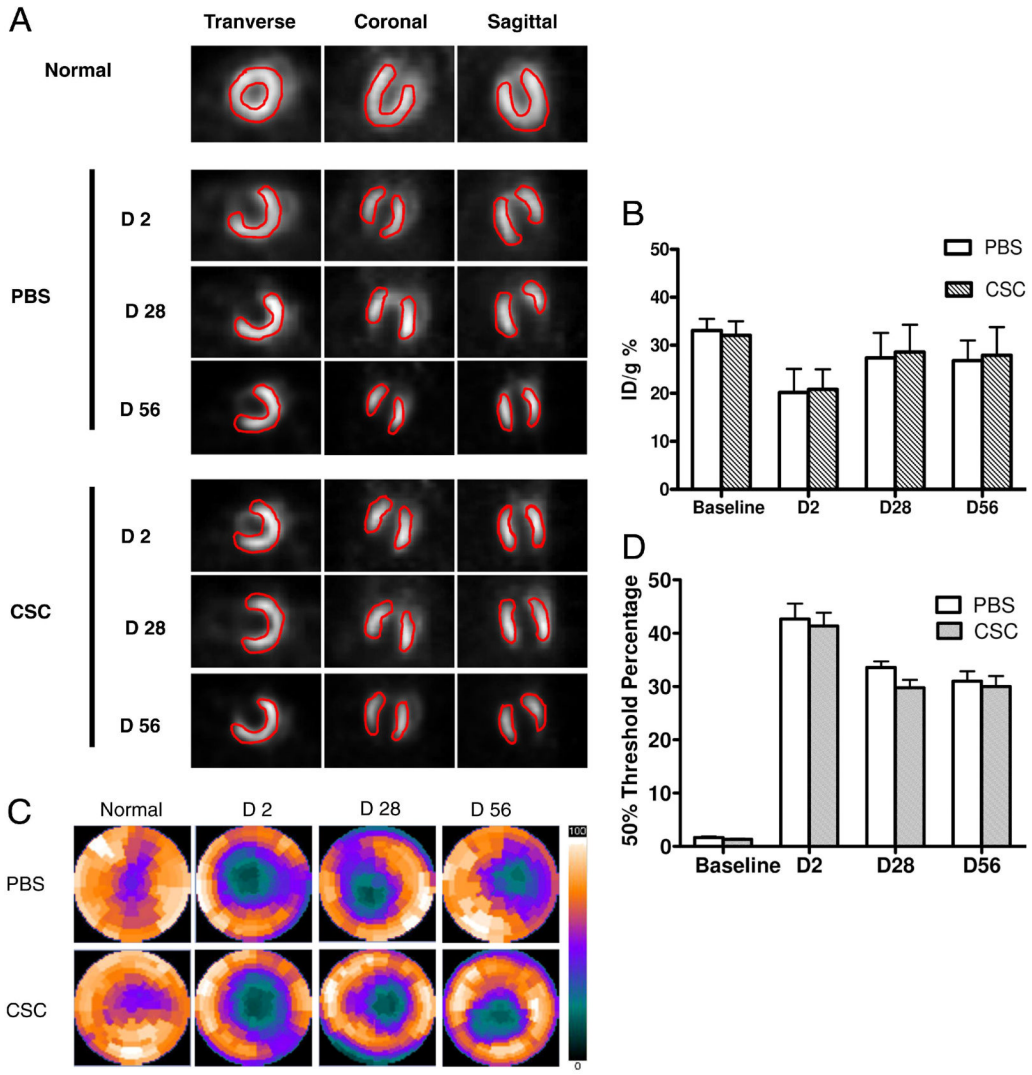

Figure 6. [^{18}F]-FDG PET imaging of cardiac viability

(A) Representative image in a normal mouse heart and at day 2, day 28, and day 56 in infarcted hearts receiving PBS vs. CSCs. **P*=0.46 and *P*=0.38 vs. PBS group at day 28 and day 56 respectively. **(B)** Detailed quantitative analysis of signals from all animals transplanted with CSCs and PBS group. There is no significant difference of the FDG uptake (% ID/g) between the two groups. **P*=0.31 and *P*=0.40 vs. PBS group at day 28 and day 56 respectively. **(C–D)** Representative polar map of the microPET images obtained from mice treated with PBS vs. CSC. Measurements are based on 50% thresholds.

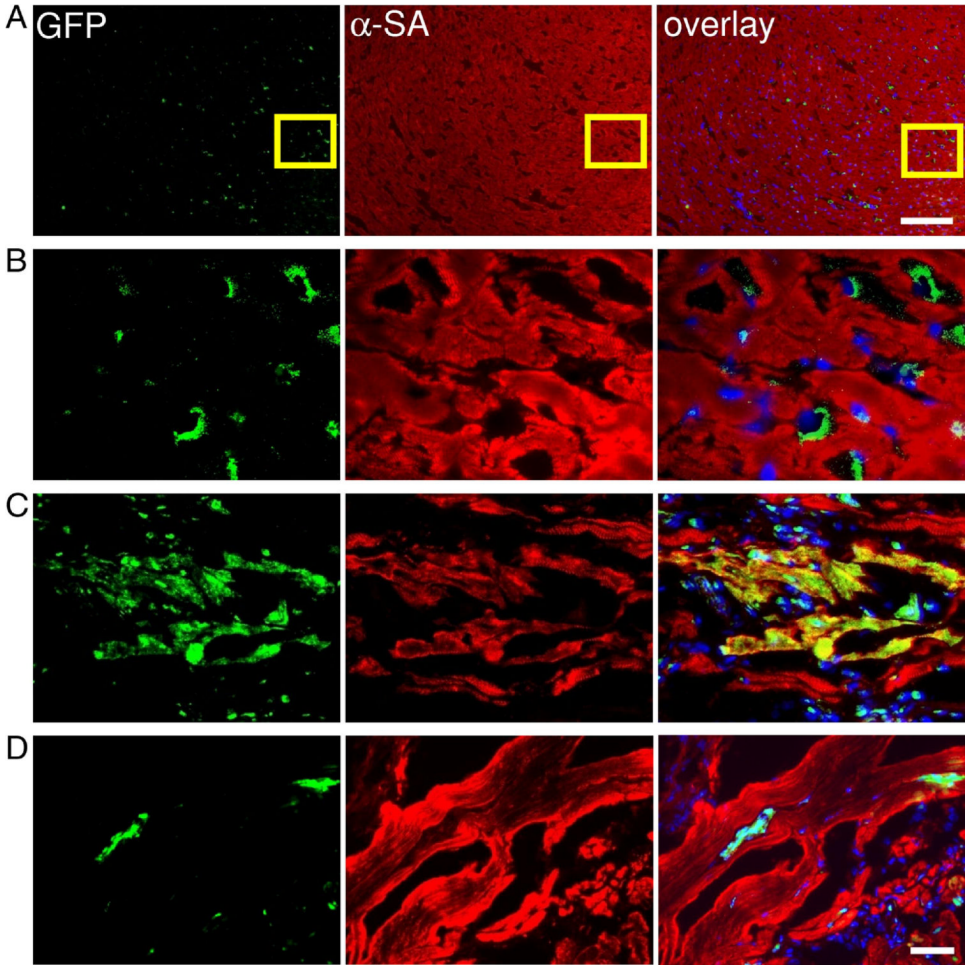

Figure 7. Tracking of grafted CSCs by immunofluorescence

(A – B) CSCs within the recipient myocardium 3 days after injection shown at low and high magnification. **(C–D)** Transplanted CSCs can differentiate and integrate with host myocardium as confirmed by GFP and α-sarcomeric actin (α-SA) double staining. At day 14, CSCs could differentiate into cardiomyocytes as confirmed by α-SA and GFP double stainings (Figure 7C). However, this population became significantly decreased when the tissues were examined at day 28 (Figure 7D), which is also consistent with the decrease in bioluminescence signals over this period of time. Scale bar=100μm (A), 20μm (B, C, D).